Time migration velocity analysis by velocity continuation[a]

[a]Published in Geophysics, 68, 1662-1672 (2003)

Sergey Fomel[1]

ABSTRACT

Time migration velocity analysis can be performed by velocity continuation, an incremental process that transforms migrated seismic sections according to changes in the migration velocity. Velocity continuation enhances residual normal moveout correction by properly taking into account both vertical and lateral movements of events on seismic images. Finite-difference and spectral algorithms provide efficient practical implementations for velocity continuation. Synthetic and field data examples demonstrate the performance of the method and confirm theoretical expectations.

INTRODUCTION

Migration velocity analysis is a routine part of prestack time migration applications. It serves both as a tool for velocity estimation (Deregowski, 1990) and as a tool for optimal stacking of migrated seismic sections prior to modeling zero-offset data for depth migration (Kim et al., 1997). In the most common form, migration velocity analysis amounts to residual moveout correction on CIP (common image point) gathers. However, in the case of dipping reflectors, this correction does not provide optimal focusing of reflection energy, since it does not account for lateral movement of reflectors caused by the change in migration velocity. In other words, different points on a stacking hyperbola in a CIP gather can correspond to different reflection points at the actual reflector. The situation is similar to that of the conventional normal moveout (NMO) velocity analysis, where the reflection point dispersal problem is usually overcome with the help of dip moveout (Deregowski, 1986; Hale, 1991). An analogous correction is required for optimal focusing in the post-migration domain. In this paper, I propose and test velocity continuation as a method of migration velocity analysis. The method enhances the conventional residual moveout correction by taking into account lateral movements of migrated reflection events.

Velocity continuation is a process of transforming time migrated images according to the changes in migration velocity. This process has wave-like properties, which have been described in earlier papers (Fomel, 1994, 1997, 2003). Hubral et al. (1996)

[1]**e-mail:** sergey@sep.stanford.edu

and Schleicher et al. (1997) use the term *image waves* to describe a similar concept. Adler (2000, 2002) generalizes the velocity continuation approach for the case of variable background velocities, using the term *Kirchhoff image propagation*. Although the velocity continuation concept is tailored for time migration, it finds important applications in depth migration velocity analysis by recursive methods (Biondi and Sava, 1999; Vaillant et al., 2000).

Applying velocity continuation to migration velocity analysis involves the following steps:

1. prestack common-offset (and common-azimuth) migration - to generate the initial data for continuation,
2. velocity continuation with stacking and semblance analysis across different offsets - to transform the offset data dimension into the velocity dimension,
3. picking the optimal velocity and slicing through the migrated data volume - to generate an optimally focused image.

The first step transforms the data to the image space. The regularity of this space can be exploited for devising efficient algorithms for the next two steps. The idea of slicing through the velocity space goes back to the work of Shurtleff (1984), Fowler (1984, 1988), and Mikulich and Hale (1992). While the previous slicing methods constructed the velocity space by repeated migration with different velocities, velocity continuation navigates directly in the migration velocity space without returning to the original data. This leads to both more efficient algorithms and a better understanding of the theoretical continuation properties (Fomel, 2003).

In this paper, I demonstrate all three steps, using both synthetic data and a North Sea dataset. I introduce and exemplify two methods for the efficient practical implementation of velocity continuation: the finite-difference method and the Fourier spectral method. The Fourier method is recommended as optimal in terms of the accuracy versus efficiency trade-off. Although all the examples in this paper are two-dimensional, the method easily extends to 3-D under the assumption of common-azimuth geometry (one oriented offset). More investigation may be required to extend the method to the multi-azimuth case.

It is also important to note that although the velocity continuation result could be achieved in principle by using prestack residual migration in Kirchhoff (Etgen, 1990) or frequency-wavenumber (Stolt, 1996) formulation, the first is inferior in efficiency, and the second is not convenient for the conventional velocity analysis across different offsets, because it mixes them in the Fourier domain (Sava, 2000). Fourier-domain angle-gather analysis (Sava et al., 2001; Sava and Fomel, 2003) opens new possibilities for the future development of the Fourier-domain velocity continuation. New insights into the possibility of extending the method to depth migration can follow from the work of Adler (2002).

NUMERICAL VELOCITY CONTINUATION IN THE POST-STACK DOMAIN

The post-stack velocity continuation process is governed by a partial differential equation in the domain, composed by the seismic image coordinates (midpoint x and vertical time t) and the additional velocity coordinate v. Neglecting some amplitude-correcting terms (Fomel, 2003), the equation takes the form (Claerbout, 1986)

$$\frac{\partial^2 P}{\partial v\, \partial t} + v\, t\, \frac{\partial^2 P}{\partial x^2} = 0 \ . \tag{1}$$

Equation (1) is linear and belongs to the hyperbolic type. It describes a wave-type process with the velocity v acting as a propagation variable. Each constant-v slice of the function $P(x,t,v)$ corresponds to an image with the corresponding constant velocity. The necessary boundary and initial conditions are

$$P|_{t=T} = 0 \qquad P|_{v=v_0} = P_0(x,t) \ , \tag{2}$$

where v_0 is the starting velocity, $T=0$ for continuation to a smaller velocity and T is the largest time on the image (completely attenuated reflection energy) for continuation to a larger velocity. The first case corresponds to "modeling" (demigration); the latter case, to seismic migration.

Mathematically, equations (1) and (2) define a Goursat-type problem (Courant and Hilbert, 1989). Its analytical solution can be constructed by a variation of the Riemann method in the form of an integral operator (Fomel, 1994, 2003):

$$P(t,x,v) = \frac{1}{(2\,\pi)^{m/2}} \int \frac{1}{(\sqrt{v^2-v_0^2}\,\rho)^{m/2}} \left(-\frac{\partial}{\partial t_0}\right)^{m/2} P_0\left(\frac{\rho}{\sqrt{v^2-v_0^2}}, x_0\right) dx_0 \ , \tag{3}$$

where $\rho = \sqrt{(v^2-v_0^2)\,t^2 + (x-x_0)^2}$, $m=1$ in the 2-D case, and $m=2$ in the 3-D case. In the case of continuation from zero velocity $v_0=0$, operator (3) is equivalent (up to the amplitude weighting) to conventional Kirchoff time migration (Schneider, 1978). Similarly, in the frequency-wavenumber domain, velocity continuation takes the form

$$\hat{P}(\omega,k,v) = \hat{P}_0(\sqrt{\omega^2 + k^2(v^2-v_0^2)}, k) \ , \tag{4}$$

which is equivalent (up to scaling coefficients) to Stolt migration (Stolt, 1978), regarded as the most efficient constant-velocity migration method.

If our task is to create many constant-velocity slices, there are other ways to construct the solution of problem (1-2). Two alternative approaches are discussed in the next two subsections.

Finite-difference approach

The differential equation (1) has a mathematical form analogous to that of the 15-degree wave extrapolation equation (Claerbout, 1976). Its finite-difference implementation, first described by Claerbout (1986) and Li (1986), is also analogous to that of

the 15-degree equation, except for the variable coefficients. One can write the implicit unconditionally stable finite-difference scheme for the velocity continuation equation in the form

$$(\mathbf{I} + a_{j+1}^{i+1}\,\mathbf{T})\,\mathbf{P}_{j+1}^{i+1} - (\mathbf{I} - a_{j}^{i+1}\,\mathbf{T})\,\mathbf{P}_{j}^{i+1} - (\mathbf{I} - a_{j+1}^{i}\,\mathbf{T})\,\mathbf{P}_{j+1}^{i} + (\mathbf{I} + a_{j}^{i}\,\mathbf{T})\,\mathbf{P}_{j}^{i} = 0\ , \quad (5)$$

where index i corresponds to the time dimension, index j corresponds to the velocity dimension, $\mathbf{P}$ is a vector along the midpoint direction, $\mathbf{I}$ is the identity matrix, $\mathbf{T}$ represents the finite-difference approximation to the second-derivative operator in midpoint, and $a_j^i = v_j\,t_i\,\Delta v\,\Delta t$.

In the two-dimensional case, equation 5 reduces to a tridiagonal system of linear equations, which can be easily inverted. In 3-D, a straightforward extension can be obtained by using either directional splitting or helical schemes (Rickett et al., 1998). The direction of stable propagation is either forward in velocity and backward in time or backward in velocity and forward in time as shown in Figure 1.

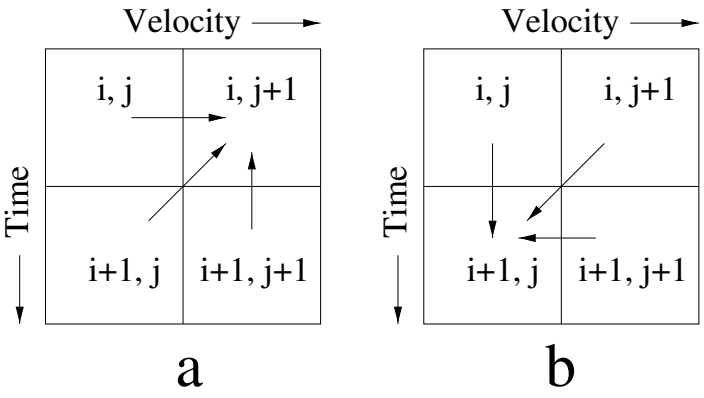

Figure 1: Finite-difference scheme for the velocity continuation equation. A stable propagation is either forward in velocity and backward in time (a) or backward in velocity and forward in time (b).

In order to test the performance of the finite-difference velocity continuation method, I use a simple synthetic model from Claerbout (1995). The reflectivity model is shown in Figure 2. It contains several features that challenge the migration performance: dipping beds, unconformity, syncline, anticline, and fault. The velocity is taken to be constant $v = 1.5\,\mathrm{km/s}$.

Figures 3–6(b) compare invertability of different migration methods. In all cases, constant-velocity modeling (demigration) was followed by migration with the correct velocity. Figures 3 and 4 show the results of modeling and migration with the Kirchhoff (Schneider, 1978) and f-k (Stolt, 1978) methods, respectively. These figures should be compared with Figure 5, showing the analogous result of the finite-difference velocity continuation. The comparison reveals a remarkable invertability of velocity continuation, which reconstructs accurately the main features and frequency content of the model. Since the forward operators were different for different migrations, this comparison did not test the migration properties themselves. For such a test, I compare the results of the Kirchhoff and velocity-continuation migrations after Stolt modeling. The result of velocity continuation, shown in Figure 6, is noticeably more accurate than that of the Kirchhoff method.

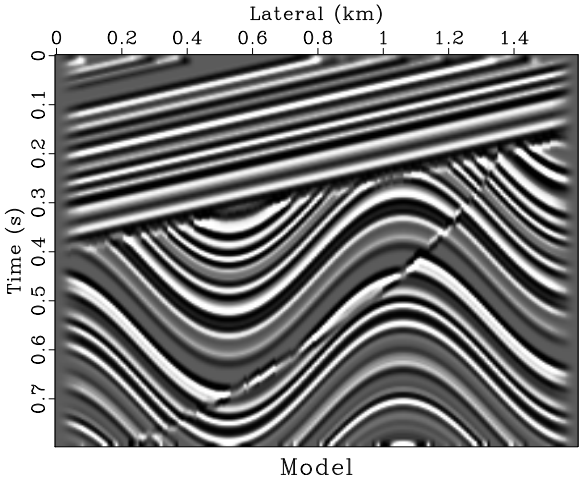

Figure 2: Synthetic model for testing finite-difference migration by velocity continuation.

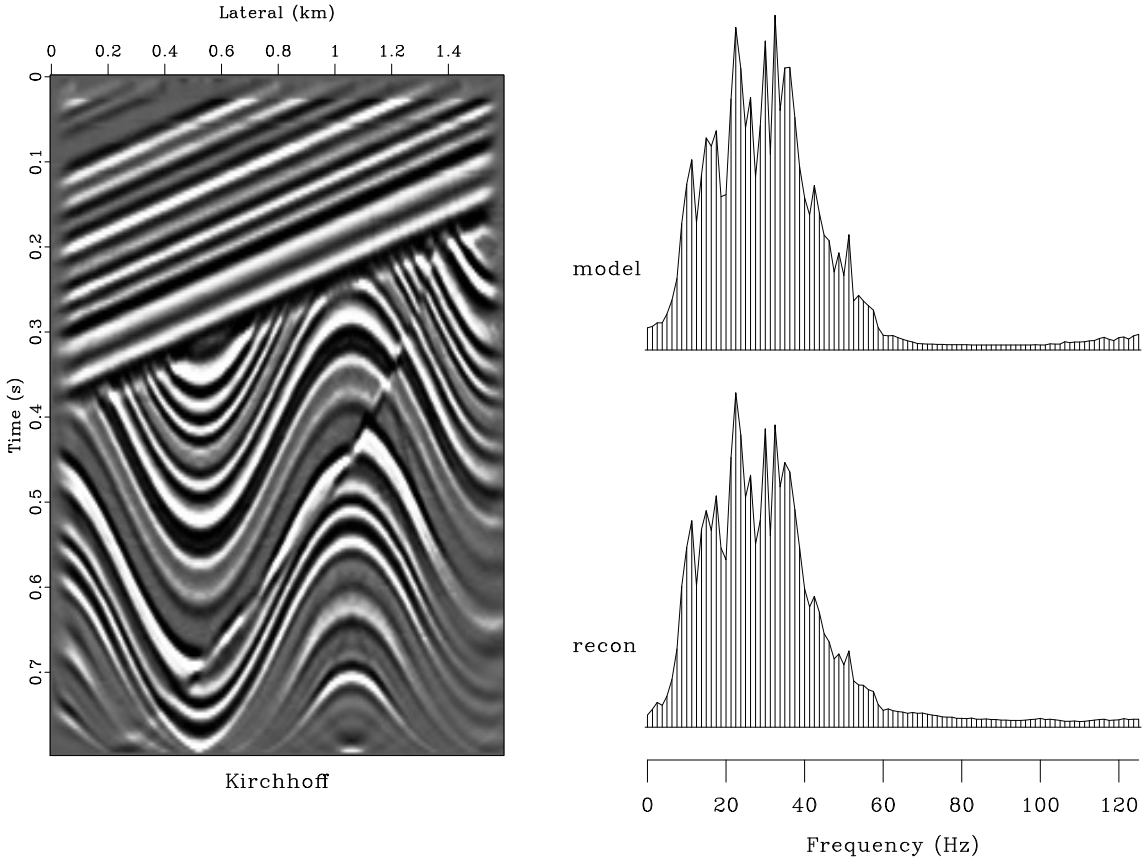

Figure 3: Result of modeling and migration with the Kirchhoff method. Top left plot shows the reconstructed model. Top right plot compares the average amplitude spectrum of the true model with that of the reconstructed image. Bottom left is the reconstruction error. Bottom right is the absolute error in the spectrum.

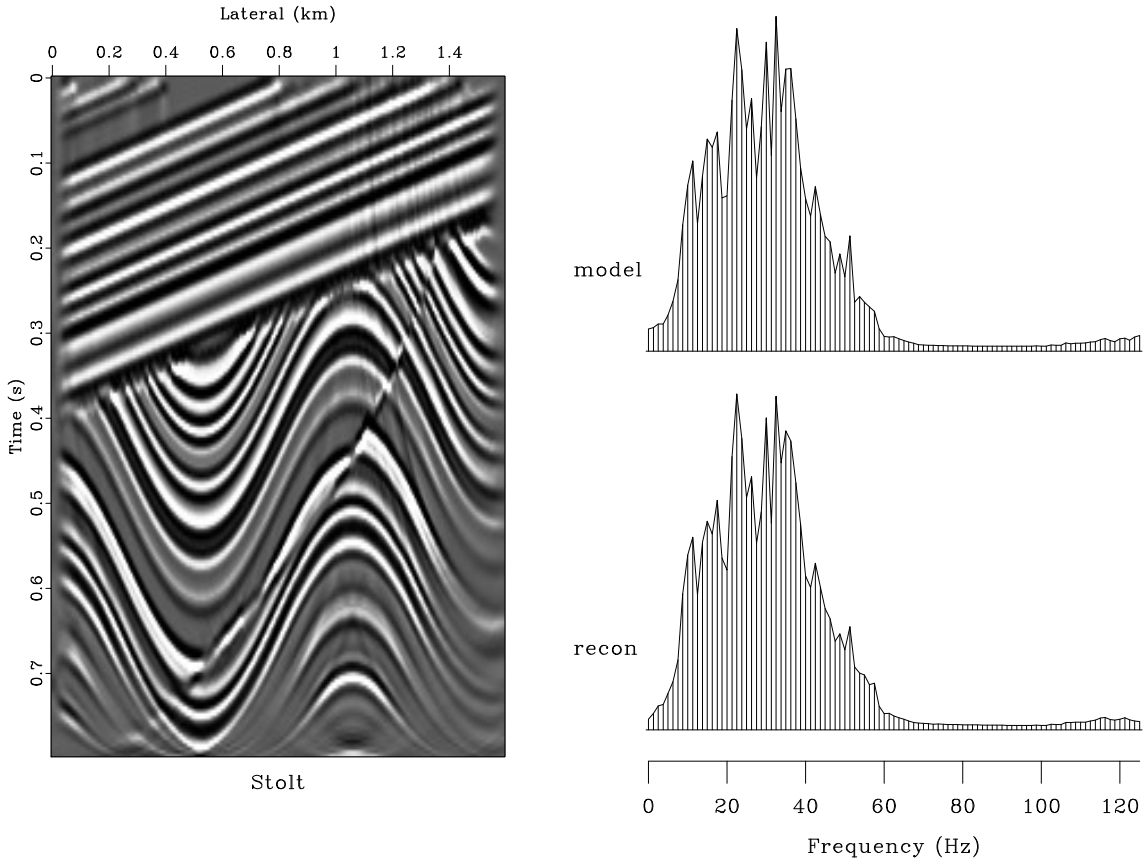

Figure 4: Result of modeling and migration with the Stolt method. Top left plot shows the reconstructed model. Top right plot compares the average amplitude spectrum of the true model with that of the reconstructed image. Bottom left is the reconstruction error. Bottom right is the absolute error in the spectrum.

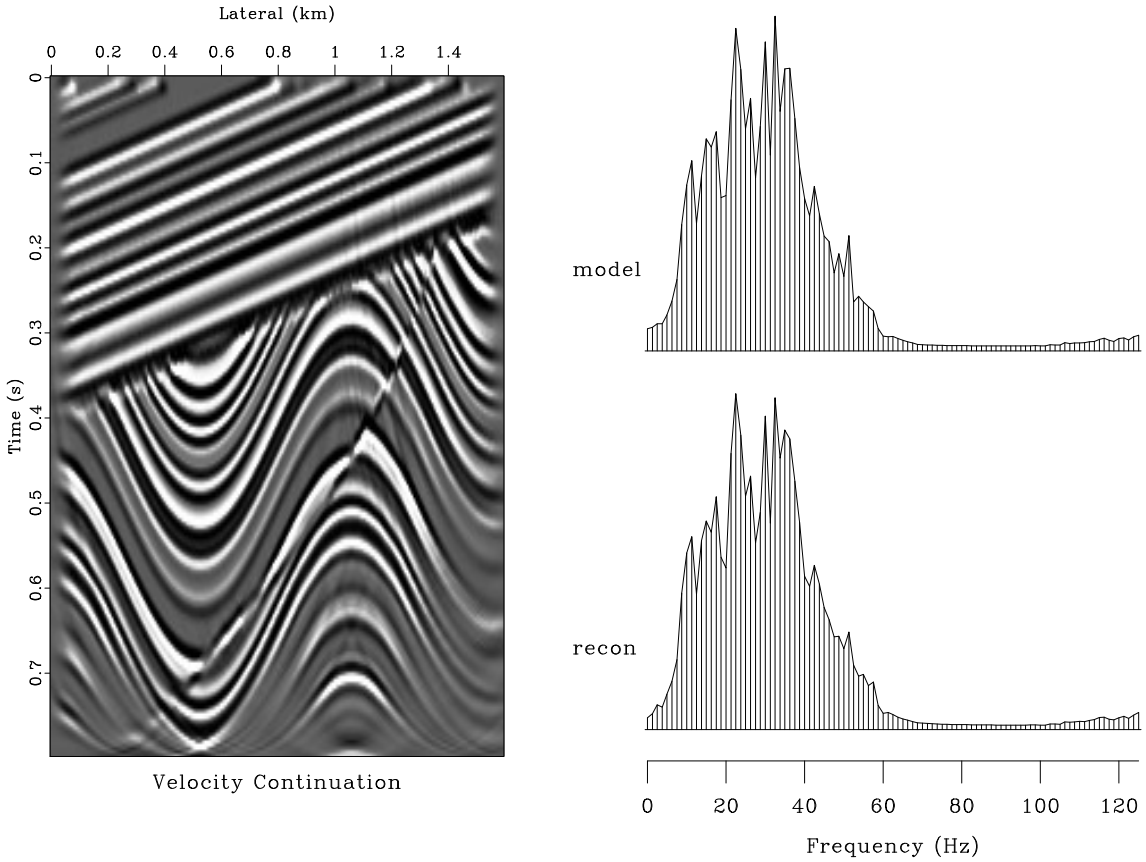

Figure 5: Result of modeling and migration with the finite-difference velocity continuation. Top left plot shows the reconstructed model. Top right plot compares the average amplitude spectrum of the true model with that of the reconstructed image. Bottom left is the reconstruction error. Bottom right is the absolute error in the spectrum.

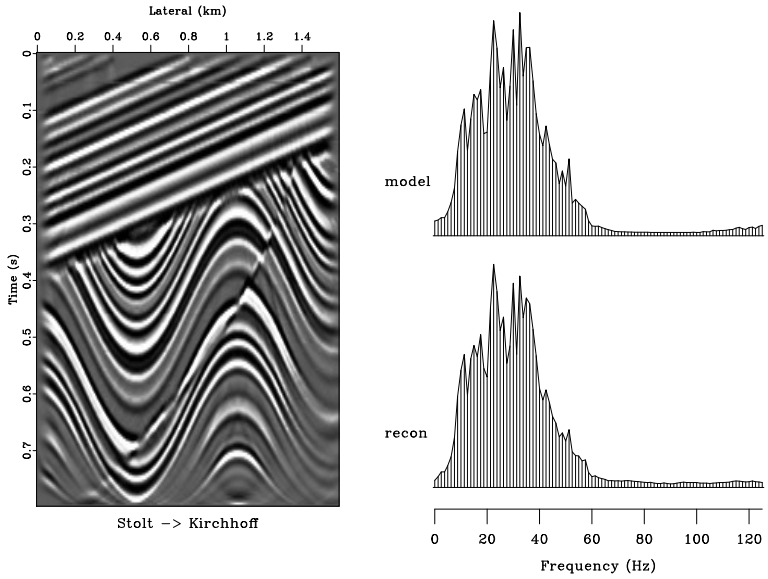

(a)

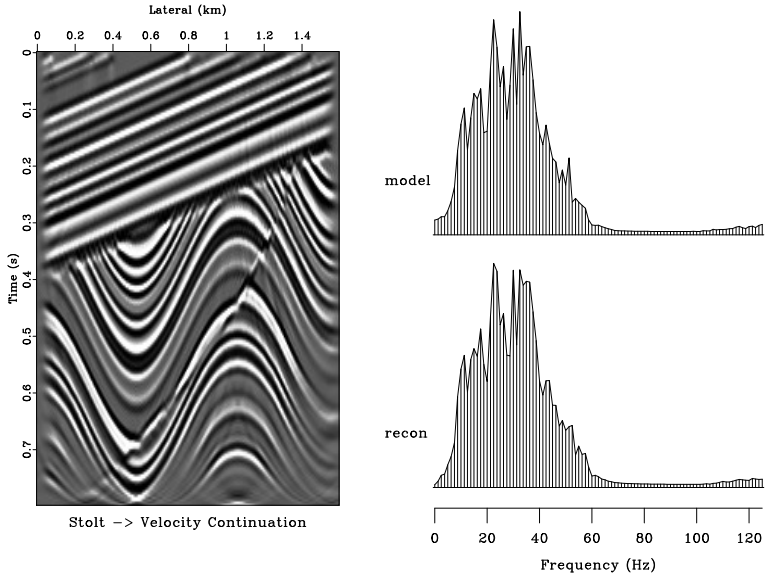

(b)

Figure 6: (a) Modeling with Stolt method, migration with the Kirchhoff method. (b) Modeling with Stolt method, migration with the finite-difference velocity continuation. Left plots show the reconstructed models. Right plots show the reconstruction errors.

These tests confirm that finite-difference velocity continuation is an attractive migration method. It possesses remarkable invertability properties, which may be useful in applications that require inversion. While the traditional migration methods transform the data between two completely different domains (data-space and image-space), velocity continuation accomplishes the same transformation by propagating the data in the extended domain along the velocity direction. Inverse propagation restores the original data. According to Li (1986), the computational speed of this method compares favorably with that of Stolt migration. The advantage is apparent for cascaded migration or migration with multiple velocity models. In these cases, the cost of Stolt migration increases in direct proportion to the number of velocity models, while the cost of velocity continuation stays the same.

Fourier approach

The change of variable $\sigma = t^2$ transforms equation (1) to the form

$$2\,\frac{\partial^2 P}{\partial v\,\partial \sigma} + v\,\frac{\partial^2 P}{\partial x^2} = 0\;, \tag{6}$$

whose coefficients do not depend on the time variables. Double Fourier transform in σ and x further simplifies equation (6) to the ordinary differential equation

$$2\,i\Omega\,\frac{d\hat{P}}{dv} - v\,k^2\,\hat{P} = 0\;, \tag{7}$$

where the "frequency" variable Ω corresponds to the stretched time coordinate σ, and k is the wavenumber in x:

$$\hat{P}(k,\Omega,v) = \iint P(x,t,v)\,e^{-i\,\Omega\,t^2 + i\,k\,x} dx\,dt \tag{8}$$

Equation (7) has an explicit analytical solution

$$\hat{P}(k,\Omega,v) = \hat{P}_0(k,\Omega)\,e^{\frac{ik^2(v_0^2 - v^2)}{4\Omega}}\;, \tag{9}$$

which leads to a very simple algorithm for the numerical velocity continuation. The algorithm consists of the following steps:

1. Input the zero-offset (post-stack) data migrated with velocity v_0 (or unmigrated if $v_0 = 0$).
2. Transform the input from a regular grid in t to a regular grid in σ.
3. Apply Fast Fourier Transform (FFT) in x and σ.
4. Multiply by the all-pass phase-shift filter $e^{\frac{ik^2(v_0^2 - v^2)}{4\Omega}}$.

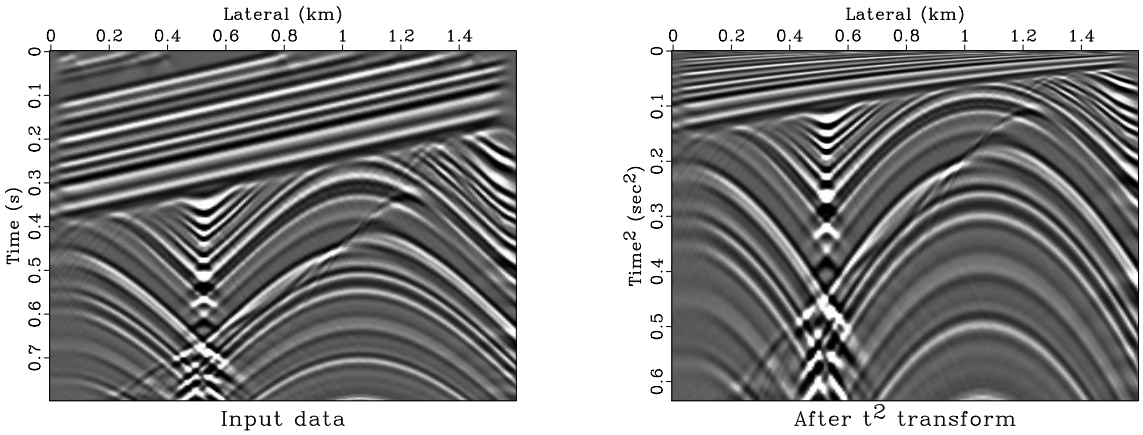

Figure 7: Synthetic seismic data before (left) and after (right) transformation to the σ grid.

5. Inverse FFT in x and σ.

6. Inverse transform to a regular grid in t.

Figure 7 shows a simple synthetic model of seismic reflection data generated from the model in Figure 2 before and after transforming the grid, regularly spaced in t, to a grid, regular in σ. The left plot of Figure 8 shows the Fourier transform of the data. Except for the nearly vertical event, which corresponds to a stack of parallel layers in the shallow part of the data, the data frequency range is contained near the origin in the $\Omega - k$ space. The right plot of Figure 8 shows the phase-shift filter for continuation from zero imaging velocity (which corresponds to unprocessed data) to the velocity of 1 km/sec. The rapidly oscillating part (small frequencies and large wavenumbers) is exactly in the region, where the data spectrum is zero. It corresponds to physically impossible reflection events.

The described algorithm is very attractive from the practical point of view because of its efficiency (based on the FFT algorithm). The operation count is roughly the same as in the Stolt migration implemented with equation (4): two forward and inverse FFTs and forward and inverse grid transform with interpolation (one complex-number transform in the case of Stolt migration). The velocity continuation algorithm can be more efficient than the Stolt method because of the simpler structure of the innermost loop (step 4 in the algorithm).

NUMERICAL VELOCITY CONTINUATION IN THE PRESTACK DOMAIN

To generalize the algorithm of the previous section to the prestack case, it is first necessary to include the residual NMO term (Fomel, 2003). Residual normal moveout

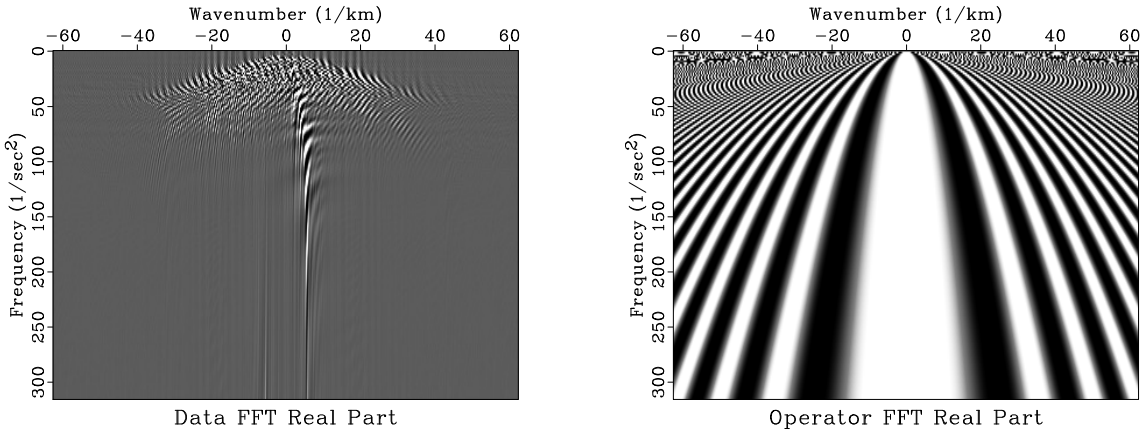

Figure 8: Left: the real part of the data Fourier transform. Right: the real part of the velocity continuation operator (continuation from 0 to 1 km/s) in the Fourier domain.

can be formulated with the help of the differential equation:

$$\frac{\partial P}{\partial v} + \frac{h^2}{v^3\, t}\,\frac{\partial P}{\partial t} = 0 \;, \tag{10}$$

where h stands for the half-offset. The analytical solution of equation (10) has the form of the residual NMO operator:

$$P(t,h,v) = P_0\left(\sqrt{t^2 + h^2\,\left(\frac{1}{v_0^2} - \frac{1}{v^2}\right)}, h\right) \;. \tag{11}$$

After transforming to the squared time $\sigma = t^2$ and the corresponding Fourier frequency Ω, equation (10) takes the form of the ordinary differential equation

$$\frac{d\hat{P}}{dv} + i\Omega\,\frac{2\,h^2}{v^3}\,\hat{P} = 0 \tag{12}$$

with the analytical frequency-domain phase-shift solution

$$\hat{P}(\Omega,h,v) = \hat{P}_0(\Omega,h)e^{\,i\,\Omega\,h^2\left(\frac{1}{v_0^2}-\frac{1}{v^2}\right)} \;. \tag{13}$$

To obtain a Fourier-domain prestack velocity continuation algorithm, one just needs to combine the phase-shift operators in equations (9) and (13) and to include stacking across different offsets. The exact velocity continuation theory also includes the residual DMO term (Fomel, 2003), which has a second-order effect, pronounced only at small depths. It is neglected here for simplicity. The algorithm takes the following form:

1. Input a set of common-offset images, migrated with velocity v_0.

2. Transform the time axis t to the squared time coordinate: $\sigma = t^2$.

3. Apply a fast Fourier transform (FFT) on both the squared time and the midpoint axis. The squared time σ transforms to the frequency Ω, and the midpoint coordinate x transforms to the wavenumber k.

4. Apply a phase-shift operator to transform to different velocities v:

$$\hat{P}(\Omega, k, v) = \sum_h \hat{P}_0(\Omega, k, h)\, e^{i \frac{k^2 \left(v_0^2 - v^2\right)}{4\,\Omega} + i\,\Omega\, h^2 \left(\frac{1}{v_0^2} - \frac{1}{v^2}\right)} \quad . \tag{14}$$

   To save memory, the continuation step is immediately followed by stacking. For velocity analysis purposes, a semblance measure (Neidell and Taner, 1971) is computed in addition to the simple stack analogously to the standard practice of stacking velocity analysis.

   Implementing the residual moveout correction in the Fourier domain allows one to package it conveniently with the phase-shift operator without the need to transform the continuation result back to the time domain. The offset dimension in equation (14) is replaced by the velocity dimension similarly to the velocity transform of the conventional stacking velocity analysis (Yilmaz, 2001).

5. Apply an inverse FFT to transform from Ω and k to σ and x.

6. Apply an inverse time stretch to transform from σ to t.

One can design similar algorithms by using the finite difference method. Although the finite-difference approach offers a faster continuation speed, the spectral algorithm has a higher accuracy while maintaining an acceptable cost.

Figure 9 shows impulse responses of prestack velocity continuation. The input for producing this figure was a time-migrated constant-offset section, corresponding to an offset of 1 km and a constant migration velocity of 1 km/s. In full accordance with the theory (Fomel, 2003), three spikes in the input section transformed into shifted ellipsoids after continuation to a higher velocity and into shifted hyperbolas after continuation to a smaller velocity. Padding of the time axis helps to avoid the wrap-around artifacts of the Fourier method. Alternatively, one could use the artifact-free but more expensive Chebyshev spectral method (Fomel, 1998).

Velocity continuation creates a time-midpoint-velocity cube (four-dimensional for 3-D data), which is convenient for picking imaging velocities in the same way as the result of common-midpoint or common-reflection-point velocity analysis. The important difference is that velocity continuation provides an optimal focusing of the reflection energy by properly taking into account both vertical and lateral movements of reflector images with changing migration velocity. An experimental evidence for this conclusion is provided in the examples section of this paper.

The next subsection discusses the velocity picking step in more detail.

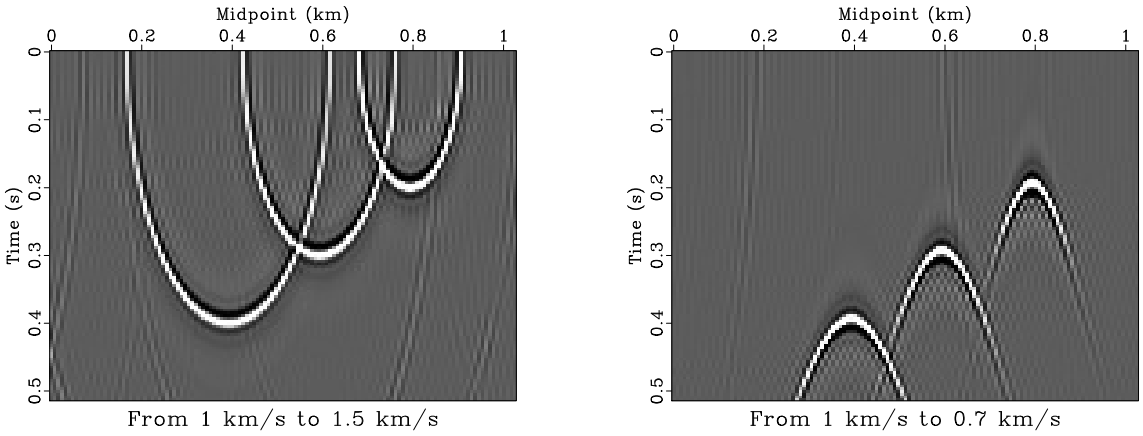

Figure 9: Impulse responses of prestack velocity continuation. Left plot: continuation from 1 km/s to 1.5 km/s. Right plot: continuation from 1 km/s to 0.7 km/s. Both plots correspond to the offset of 1 km.

Velocity picking and slicing

After the velocity continuation process has created a time-midpoint-velocity cube, one can pick the best focusing velocity from that cube and create an optimally focused image by slicing through the cube. This step is common in other methods that involve velocity slicing (Shurtleff, 1984; Fowler, 1984; Mikulich and Hale, 1992). The algorithm described below has been also adopted by Sava (2000) for velocity analysis in wave-equation migration.

A simple automatic velocity picking algorithm follows from solving the following regularized least-squares system:

$$\left\{ \begin{array}{lcl} \mathbf{W}\,\mathbf{x} & \approx & \mathbf{W}\,\mathbf{p} \\ \epsilon \mathbf{D}\mathbf{x} & \approx & \mathbf{0} \end{array} \right. . \tag{15}$$

In the more standard notation, the solution $\mathbf{x}$ minimizes the least-squares objective function

$$(\mathbf{x}-\mathbf{p})^T\,\mathbf{W}^2\,(\mathbf{x}-\mathbf{p}) + \epsilon^2\,\mathbf{x}^T\,\mathbf{D}^T\,\mathbf{D}\,\mathbf{x} \tag{16}$$

Here $\mathbf{p}$ is the vector of blind maximum-semblance picks (possibly in a predefined fairway), $\mathbf{x}$ is the estimated velocity picks, $\mathbf{W}$ is the weighting operator with the weight corresponding to the semblance values at $\mathbf{p}$, ϵ is the scalar regularization parameter, $\mathbf{D}$ is a roughening operator, and $\mathbf{D}^T$ is the adjoint operator. The first least-squares fitting goal in (15) states that the estimated velocity picks should match the measured picks where the semblance is high enough[2]. The second fitting goal tries

[2]Of course, this goal might be dangerous, if the original picks $\mathbf{p}$ include regular noise (such as multiple reflections) with high semblance value (Toldi, 1985). For simplicity, and to preserve the linearity of the problem, I assume that this is not the case.

to find the smoothest velocity function possible. The least-squares solution of problem (15) takes the form

$$\mathbf{x} = \left(\mathbf{W}^2 + \epsilon^2 \, \mathbf{D}^T \, \mathbf{D}\right)^{-1} \, \mathbf{W}^2 \, \mathbf{p} \; . \tag{17}$$

In the case of picking a one-dimensional velocity function from a single semblance panel, one can simplify the algorithm by choosing $\mathbf{D}$ to be a convolution with the derivative filter $(1, -1)$. It is easy to see that in this case the inverted matrix in formula (17) has a tridiagonal structure and therefore can be easily inverted with a linear-time algorithm. The regularization parameter ϵ controls the amount of smoothing of the estimated velocity function. Figure 10 shows an example velocity spectrum and two automatic picks for different values of ϵ.

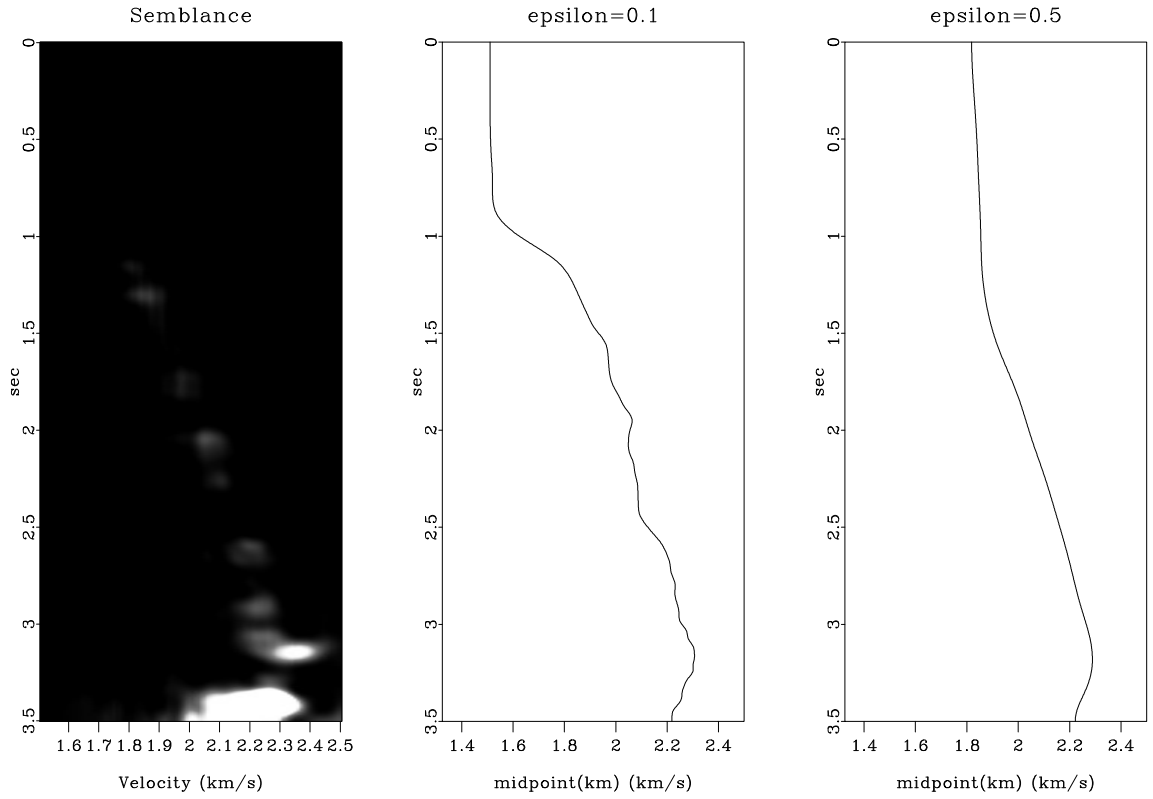

Figure 10: Semblance panel (left) and automatic velocity picks for different values of the regularization parameter. Higher values of ϵ lead to smoother velocities.

In the case of picking two- or three-dimensional velocity functions, one could generalize problem (15) by defining $\mathbf{D}$ as a 2-D or 3-D roughening operator. I chose to use a more simplistic approach, which retains the one-dimensional structure of the algorithm. I transform system (15) to the form

$$\left\{ \begin{array}{rcl} \mathbf{W}\,\mathbf{x} & \approx & \mathbf{W}\,\mathbf{p} \\ \epsilon \mathbf{D}\mathbf{x} & \approx & \mathbf{0} \\ \lambda \mathbf{x} & \approx & \lambda \mathbf{x_0} \end{array} \right. , \tag{18}$$

where $\mathbf{x}$ is still one-dimensional, and $\mathbf{x}_0$ is the estimate from the previous midpoint location. The scalar parameter λ controls the amount of lateral continuity in the estimated velocity function. The least-squares solution to system (18) takes the form

$$\mathbf{x} = \left(\mathbf{W}^2 + \epsilon^2 \, \mathbf{D}^T \, \mathbf{D} + \lambda^2 \, \mathbf{I}\right)^{-1} \left(\mathbf{W}^2 \, \mathbf{p} + \lambda^2 \mathbf{x_0}\right) \ , \tag{19}$$

where $\mathbf{I}$ denotes the identity matrix. Formula (19) also reduces to an efficient tridiagonal matrix inversion.

After the velocity has been picked, an optimally focused image is constructed by slicing in the time-midpoint-velocity cube. I used simple linear interpolation for slicing between the velocity grid values. A more accurate interpolation technique can be easily adopted.

EXAMPLES

I demonstrate the performance of the method using a simple 2-D synthetic test and a field data example from the North Sea.

Synthetic Test

The synthetic test uses constant-velocity prestack modeling and migration to check the validity of the method when all the theoretical requirements are satisfied. The data were generated from the synthetic reflectivity model (Figure 2) and included 60 offsets ranging from 0 to 0.5 km. The exact velocity in the model is 1.5 km/s, and the initial velocity for starting the continuation process was chosen at 2 km/s.

Figure 11 compares the semblance panels for migration velocity analysis using velocity continuation and using the conventional (NMO) analysis. In the top part of the image, both panels show maximum picks at the correct velocity (1.5 km/s). The advantage of velocity continuation is immediately obvious in the deeper part of the image, where the events are noticeably better focused.

The final result of velocity continuation (after picking maximum semblance and slicing in the velocity cube) is shown in the bottom left plot of Figure 12. For comparison, Figure 12 also shows the result of migration with the correct velocity (the top left plot), initial velocity (the top right plot), and the result of velocity slicing after the simple NMO correction, corresponding to the conventional MVA (the bottom right plot). The same velocity picking and slicing program was used in both cases. The comparison clearly shows that, in this simple example, velocity continuation is able to accurately reproduce the correct image without using any prior information about the migration velocity and without any need for repeating the prestack migration procedure. Velocity continuation correctly images events with conflicting dips by properly taking into account both vertical and lateral shifts in the image position.

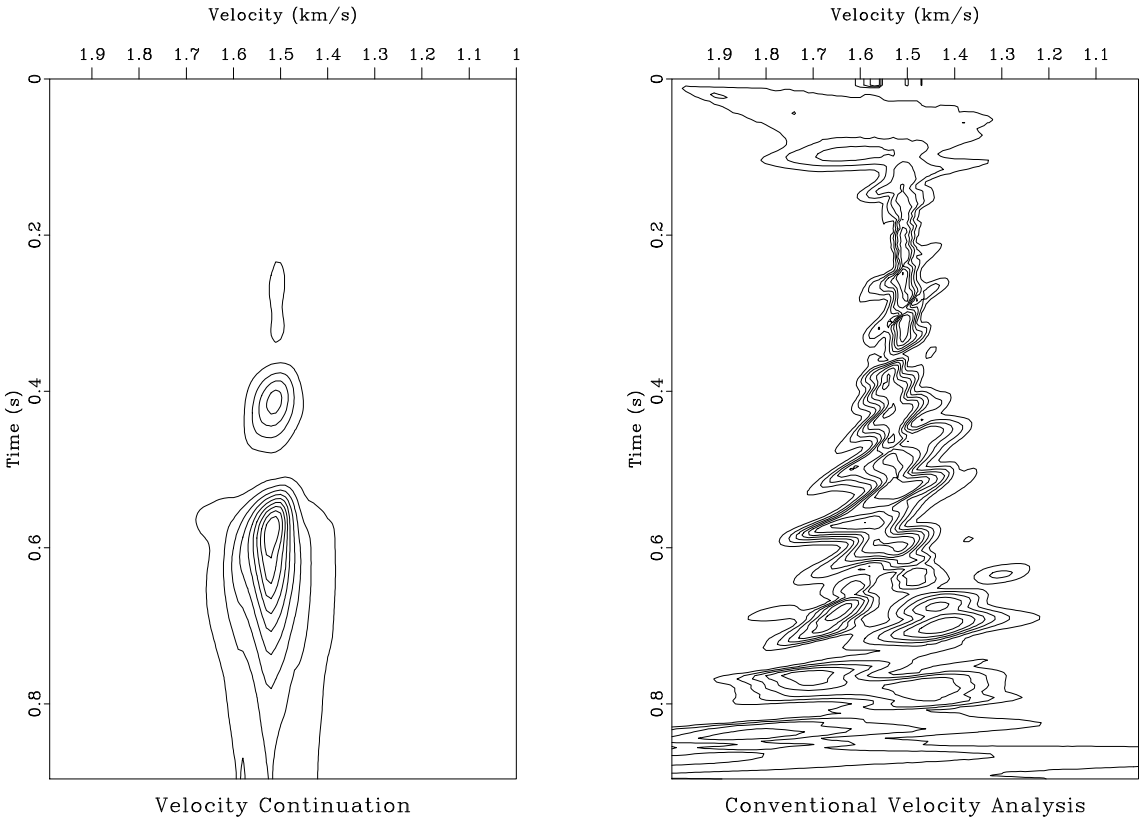

Figure 11: Semblance panels for migration velocity analysis at the common image point 1 km. Left: after velocity continuation. Right: after conventional (NMO) velocity analysis. In a structurally complex region, velocity continuation clearly provides better focusing. The correct velocity is 1.5 km/s.

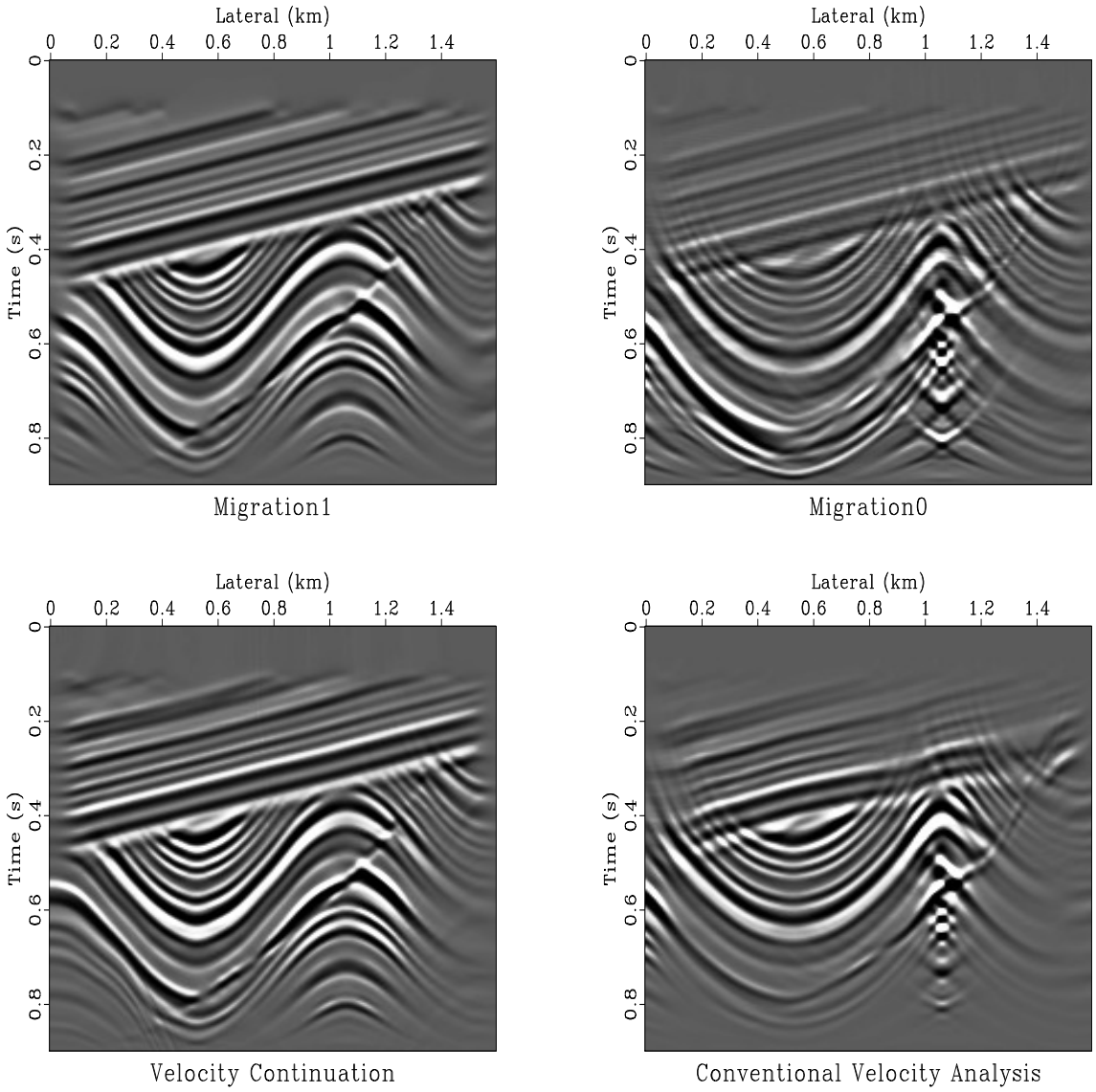

Figure 12: Velocity continuation tested on the synthetic example. Top left: prestack migration with the correct velocity of 1.5 km/s. Top right: prestack migration with the velocity of 2 km/s. Bottom left: the result of velocity continuation. Bottom right: the result from picking migration image after only conventional NMO correction.

Field Data Example

Figure 13 compares the result of a constant-velocity prestack migration with the velocity of 2 km/s, applied to a dataset from the North Sea (courtesy of Elf Aquitaine) and the result of velocity continuation to the same velocity from a migration with a smaller velocity of 1.4 km/s (Figure 13a). The two images (Figures 13b and 13c) look remarkably similar, in full accordance with the theory.

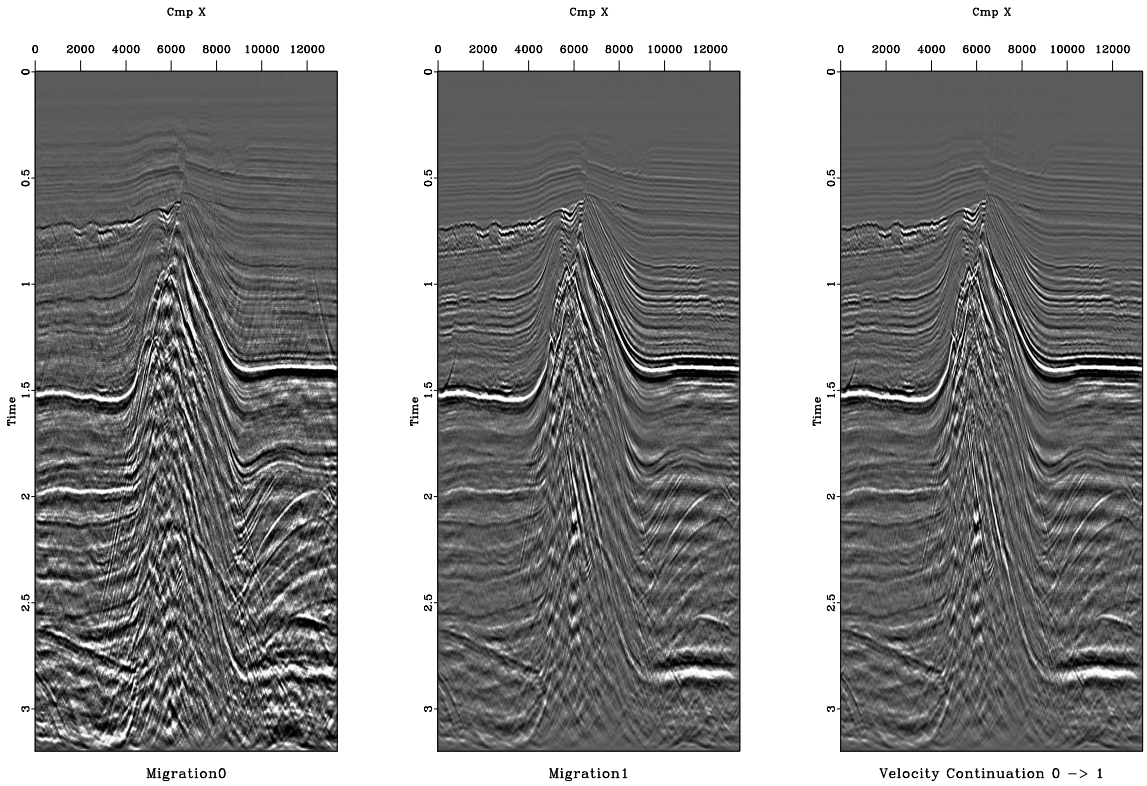

Figure 13: Constant-offset section of the North Sea dataset after migration with the velocity of 1.4 km/s (a), migration with the velocity of 2 km/s (b), migration with the velocity of 1.4 km/s and velocity continuation to 2 km/s (c).

Figure 14 shows a result of two-dimensional velocity picking after velocity continuation. I used values of $\epsilon = 0.1$ and $\lambda = 0.1$. The first parameter controls the vertical smoothing of velocities, while the second parameter controls the amount of lateral continuity.

Figure 15 shows the final result of velocity continuation: an image, obtained by slicing through the velocity cube with the picked imaging velocities. The edges of the salt body in the middle of the section have been sharply focused by the velocity continuation process. To transform the already well focused image into the depth domain, one may proceed in a way similar to *hybrid migration*: demigration to zero-offset, followed by post-stack depth migration (Kim et al., 1997). This step would require constructing an interval velocity model from the picked imaging velocities.

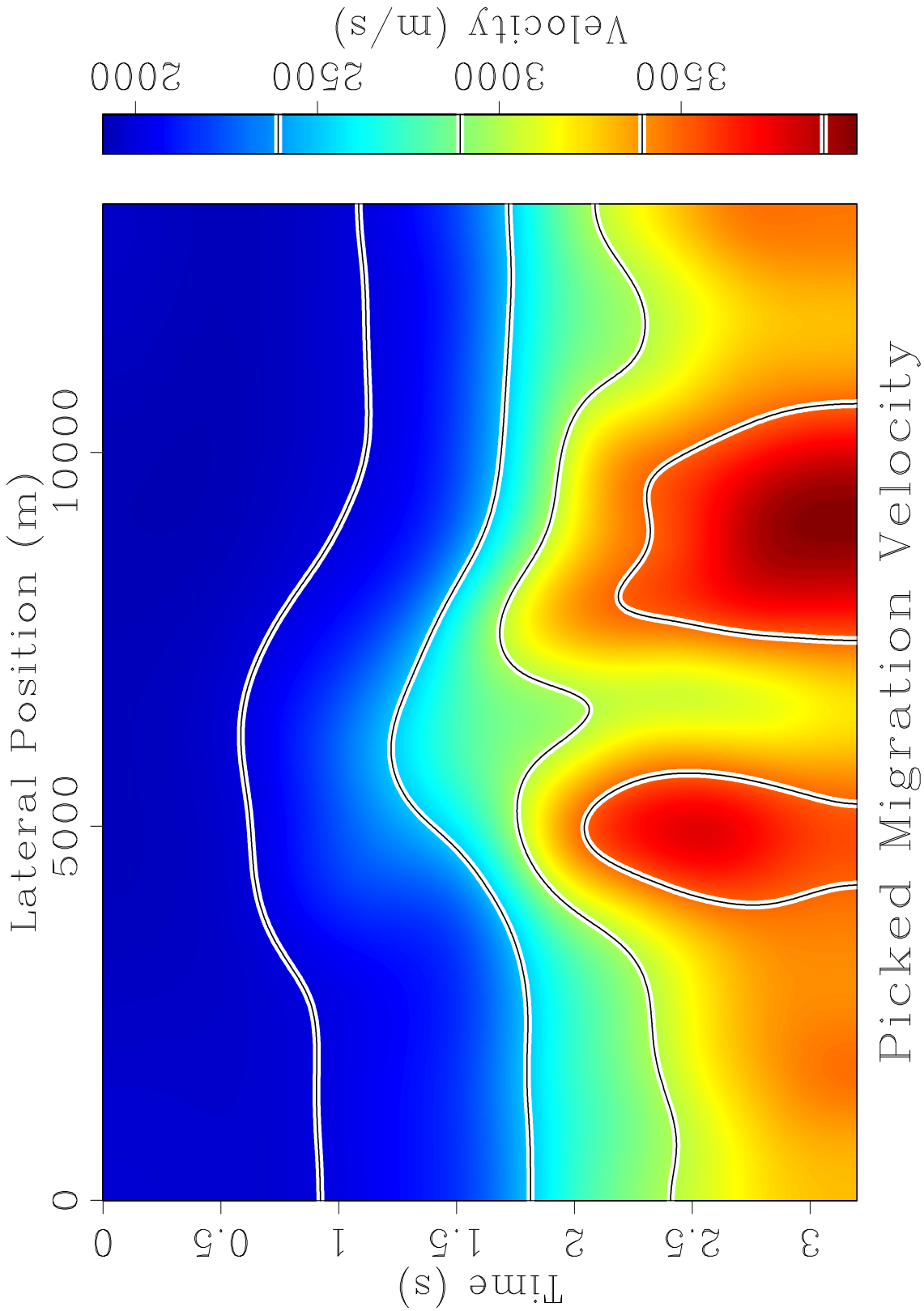

Figure 14: Automatically picked migration velocity after velocity continuation.

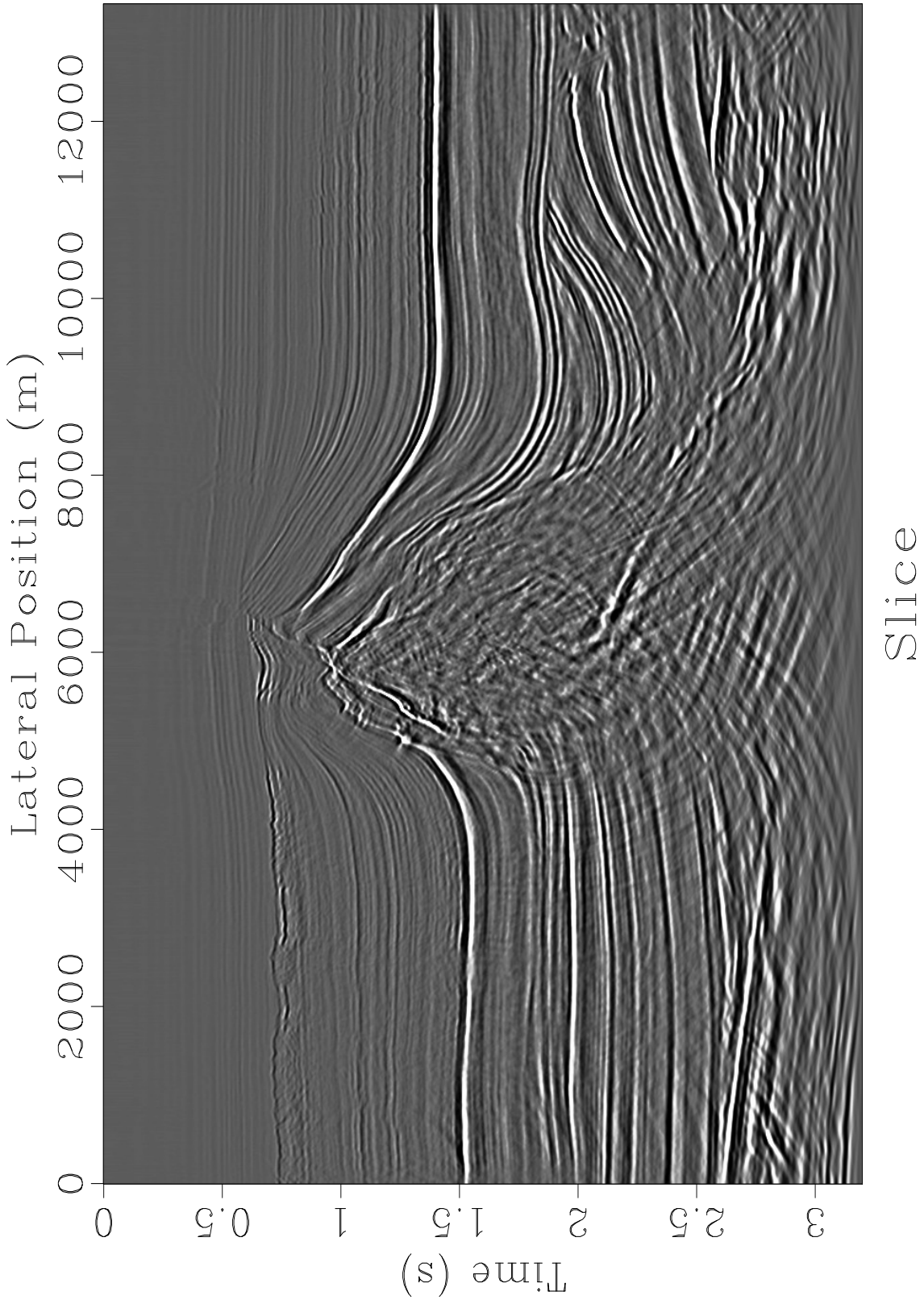

Figure 15: Final result of velocity continuation: seismic image, obtained by slicing through the velocity cube.

CONCLUSIONS

Velocity continuation is a powerful method for time migration velocity analysis. The strength of this method follows from its ability to take into account both vertical and lateral movement of the reflection events in seismic images with the changes of migration velocity.

Efficient practical algorithms for velocity continuation can be constructed using either finite-difference or spectral methods. When applied in the post-stack (zero-offset) setting, velocity continuation can be used as a computationally attractive method of time migration. Both finite-difference and spectral approaches possess remarkable invertability properties: continuation to a lower velocity reverses continuation to a higher velocity. For the finite-difference algorithm, this property is confirmed by synthetic tests. For the spectral algorithm, it follows from the fact that velocity continuation reduces to a simple phase-shift unitary operator.

Including velocity continuation in the practice of migration velocity analysis can improve the focusing power of time migration and reduce the production time by avoiding the need for iterative velocity refinement. No prior velocity model is required for this type of velocity analysis. This conclusion is confirmed by synthetic and field data examples.

ACKNOWLEDGMENTS

I thank Jon Claerbout, Biondo Biondi, and Bill Symes for useful and stimulating discussions, the sponsors of the Stanford Exploration Project for their financial support, and Elf Aquitaine for providing the data used in this work. I am also grateful to Paul Fowler, Samuel Gray, Hugh Geiger, and one anonymous reviewer for thorough and helpful reviews that improved the quality of the paper.

REFERENCES

Adler, F., 2000, Kirchhoff image propagation, *in* 70th Annual Internat. Mtg., Soc. Expl. Geophys., Expanded Abstracts: Soc. Expl. Geophys., 988–991.

———, 2002, Kirchhoff image propagation: Geophysics, **67**, 126–134.

Biondi, B., and P. Sava, 1999, Wave-equation migration velocity analysis: 69th Ann. Internat. Mtg, Soc. of Expl. Geophys., 1723–1726.

Claerbout, J., 1976, Fundamentals of geophysical data processing: Blackwell.

Claerbout, J. F., 1986, Velocity extrapolation by cascaded 15 degree migration, *in* SEP-48: Stanford Exploration Project, 79–84.

———, 1995, Basic Earth Imaging: Stanford Exploration Project.

Courant, R., and D. Hilbert, 1989, Methods of mathematical physics: John Wiley & Sons.

Deregowski, S. M., 1986, What is DmO: First Break, **04**, 7–24.

———, 1990, Common-offset migrations and velocity analysis: First Break, **08**, 224–234.

Etgen, J., 1990, Residual prestack migration and interval velocity estimation: PhD thesis, Stanford University.

Fomel, S., 1997, Velocity continuation and the anatomy of prestack residual migration: 67th Ann. Internat. Mtg, Soc. of Expl. Geophys., 1762–1765.

———, 1998, Velocity continuation by spectral methods, *in* SEP-97: Stanford Exploration Project, 157–172.

———, 2003, Velocity continuation and the anatomy of residual prestack time migration: Geophysics, submitted for publication.

Fomel, S. B., 1994, Method of velocity continuation in the problem of temporal seismic migration: Russian Geology and Geophysics, **35**, 100–111.

Fowler, P., 1984, Velocity independent imaging of seismic reflectors: 54th Ann. Internat. Mtg, Soc. of Expl. Geophys., Session:S1.8.

———, 1988, Seismic velocity estimation using prestack time migration: PhD thesis, Stanford University.

Hale, D., 1991, Course notes: Dip moveout processing: Soc. Expl. Geophys.

Hubral, P., M. Tygel, and J. Schleicher, 1996, Seismic image waves: Geophysical Journal International, **125**, 431–442.

Kim, Y. C., W. B. Hurt, L. J. Maher, and P. J. Starich, 1997, Hybrid migration: A cost-effective 3-D depth-imaging technique: Geophysics, **62**, 568–576.

Li, Z., 1986, Cascaded one step fifteen degree migration versus Stolt migration, *in* SEP-48: Stanford Exploration Project, 85 –100.

Mikulich, W., and D. Hale, 1992, Steep-dip v(z) imaging from an ensemble of Stolt-like migrations: Geophysics, **57**, 51–59.

Neidell, N. S., and M. T. Taner, 1971, Semblance and other coherency measures for multichannel data: Geophysics, **36**, 482–497.

Rickett, J., J. Claerbout, and S. B. Fomel, 1998, Implicit 3-D depth migration by wavefield extrapolation with helical boundary conditions: 68th Ann. Internat. Mtg, Soc. of Expl. Geophys., 1124–1127.

Sava, P., 2000, Prestack Stolt residual migration for migration velocity analysis: 70th

Ann. Internat. Mtg, Soc. of Expl. Geophys., 992–995.

Sava, P., B. Biondi, and S. Fomel, 2001, Amplitude-preserved common image gathers by wave-equation migration: 71st Ann. Internat. Mtg, Soc. of Expl. Geophys., 296–299.

Sava, P., and S. Fomel, 2003, Wave-equation angle-domain common-image gathers: Geophysics, in press.

Schleicher, J., P. Hubral, G. Hocht, and F. Liptow, 1997, Seismic constant-velocity remigration: Geophysics, **62**, 589–597.

Schneider, W. A., 1978, Integral formulation for migration in two-dimensions and three-dimensions: Geophysics, **43**, 49–76.

Shurtleff, R. N., 1984, An F-K procedure for prestack migration and migration velocity analysis, *in* Presented at the 46th Annual EAGE Mtg., London: EAGE.

Stolt, R. H., 1978, Migration by Fourier transform: Geophysics, **43**, 23–48. (Discussion and reply in GEO-60-5-1583).

———, 1996, Short note - A prestack residual time migration operator: Geophysics, **61**, 605–607.

Toldi, J., 1985, Velocity analysis without picking: PhD thesis, Stanford University.

Vaillant, L., H. Calandra, P. Sava, and B. Biondi, 2000, 3-D wave-equation imaging of a North Sea dataset: Common-azimuth migration + residual migration: 70th Ann. Internat. Mtg, Soc. of Expl. Geophys., 874–877.

Yilmaz, O., 2001, Seismic Data Analysis: Soc. of Expl. Geophys.